THE JOURNAL OF PHYSICAL CHEMISTRY Letters

Letter

pubs.acs.org/JPCL

Interlayer Registry to Determine the Sliding Potential of Layered Metal Dichalcogenides: The Case of *2H*-MoS_2

Adi Blumberg,[†] Uri Keshet,[†] Inbal Zaltsman,[†] and Oded Hod*

Department of Chemical Physics, School of Chemistry, The Sackler Faculty of Exact Sciences, Tel-Aviv University, Tel-Aviv 69978, Israel

Supporting Information

ABSTRACT: We provide a simple and intuitive explanation for the interlayer sliding energy landscape of metal dichalcogenides. On the basis of the recently introduced registry index (RI) concept, we define a purely geometrical parameter that quantifies the degree of interlayer commensurability in the layered phase of molybdenum disulfide (*2H*-MoS_2). A direct relation between the sliding energy landscape and the corresponding interlayer registry surface of *2H*-MoS_2 is discovered. A simple fit of the model parameters to capture the sliding energy landscape obtained at different external loads enables the identification and isolation of the prominent interlayer interactions dictating the interlayer sliding physics under different tribological scenarios. The success of our method in capturing the results of complex quantum mechanical calculations along with its high computational efficiency marks the RI as a promising tool for studying the tribology of complex nanoscale material interfaces in the wearless friction regime.

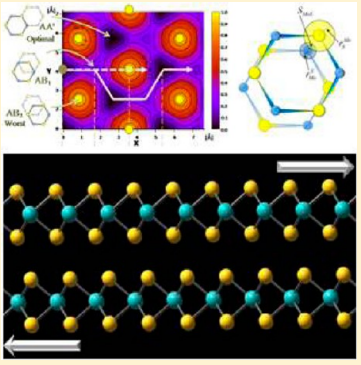

SECTION: Surfaces, Interfaces, Porous Materials, and Catalysis

Nanotribology is the science of friction, wear, and lubrication occurring at nanoscale interfaces. Such interfaces often appear in nanoelectromechanical systems (NEMS), which present the ultimate miniaturization of electromechanical devices. One of the main known caveats of NEMS is their low mechanical durability resulting from severe effects of friction and wear on systems that are characterized by a high surface-to-volume ratio. While, in principle, lubrication should reduce such effects, traditional liquid-phase lubricants usually fail to perform under nanoscale-confined conditions as they become too viscous. Thus, one of the primary goals of nanotribology is the design of new materials that will present low friction at the atomic level.

Recent experiments on pristine solid-state layered materials have shown strong dependence of their interlayer sliding friction on the misfit angle where friction was found to nearly vanish when sliding occurred out of registry.[1] This unique phenomenon, termed superlubricity,[2,3] marks layered materials as promising candidates for serving as active components in NEMS[4−13] as well as improved solid lubricants for macroscopic devices.[14−20]

Among the various members of the family of layered materials, MoS_2 and WS_2 have been long known to serve as excellent solid lubricants,[16,21−23] and MoS_2 has also recently emerged as a promising candidate for electronic components.[24−26] Despite the widespread use of these materials as lubrication additives, the experimental[20,27,28] and theoretical[21,22,29−31] study of the nanoscopic origin of their tribological behavior remains a very active field of research. Theoretical studies often rely either on molecular dynamics simulations based on appropriately parametrized force fields[21] or on first-principles calculations using advanced density functional theory approximations.[29,31] While such calculations usually result in remarkable agreement with experimental measurements, their level of complexity may shadow the relation between atomic-scale processes and collective tribological material properties. In the present Letter, we derive a simple and intuitive geometrical model that enables the characterization of the interlayer sliding energy landscape of *2H*-MoS_2 and directly relates it to the detailed atomic structure and degree of commensurability of the interface.

To this end, we utilize the registry index (RI) concept,[32] which has recently proven to be an efficient and reliable tool for quantifying the registry mismatch in bilayer systems and mimicking their corrugated sliding energy landscape.[32−34] Within this approach, each atom in the unit cell is ascribed with a circle centered around its position, and the overlaps between the projections of circles assigned to atoms located on one layer with circles associated with atoms belonging to the other layer are calculated. The obtained overlaps are appropriately summed to produce a simple numerical measure of the overall registry mismatch. This numerical value is then normalized to the range [0:1], where 0 represents perfect interlayer registry and 1 stands for the worst stacking mode in terms of the total energy. In the case of graphene and h-BN, where the sliding between two perfect two-dimensional layers is considered, a single circle is ascribed to each atomic

Received: June 6, 2012
Accepted: June 29, 2012
Published: June 29, 2012

   dx.doi.org/10.1021/jz300735v | *J. Phys. Chem. Lett.* 2012, 3, 1936−1940

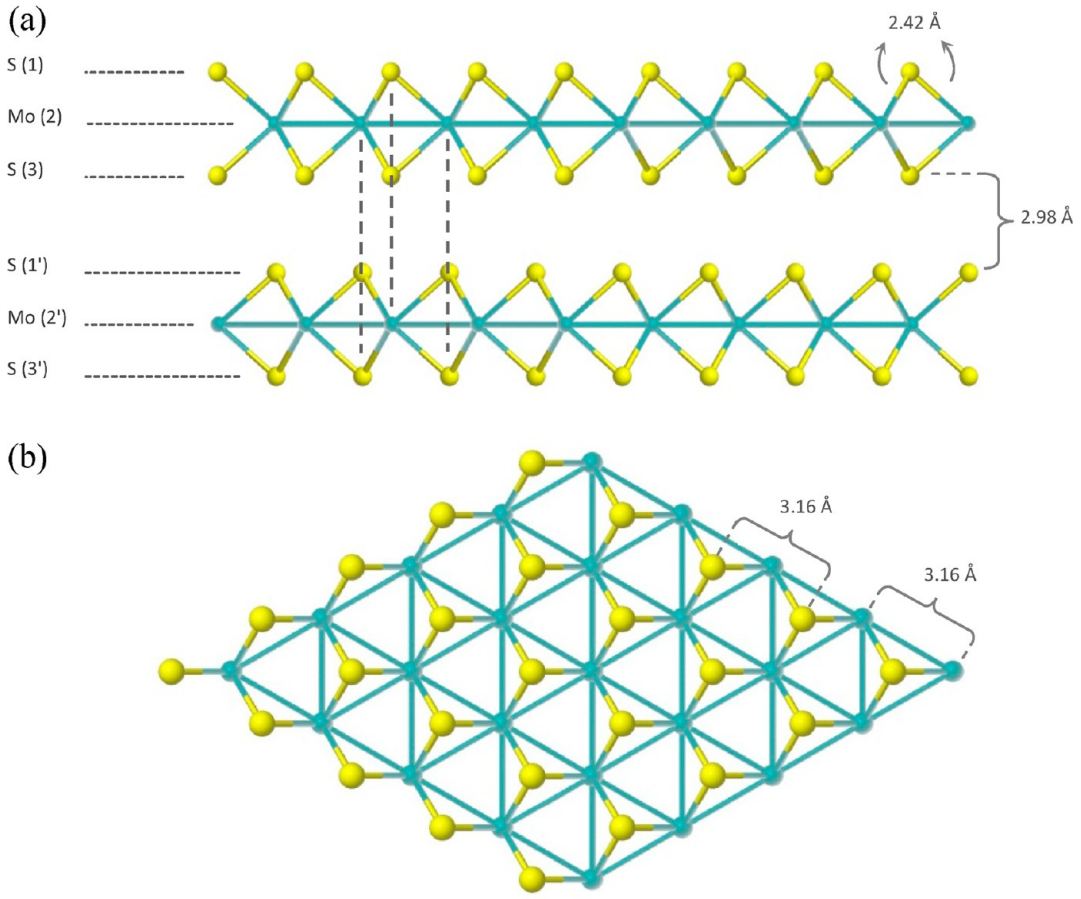

Figure 1. Crystal structure of MoS_2. (a) Side view of two layers in the optimal AA′ stacking mode, emphasizing the structure of the three sublayers. (b) Top view of a single layer showing the hexagonal crystal symmetry.

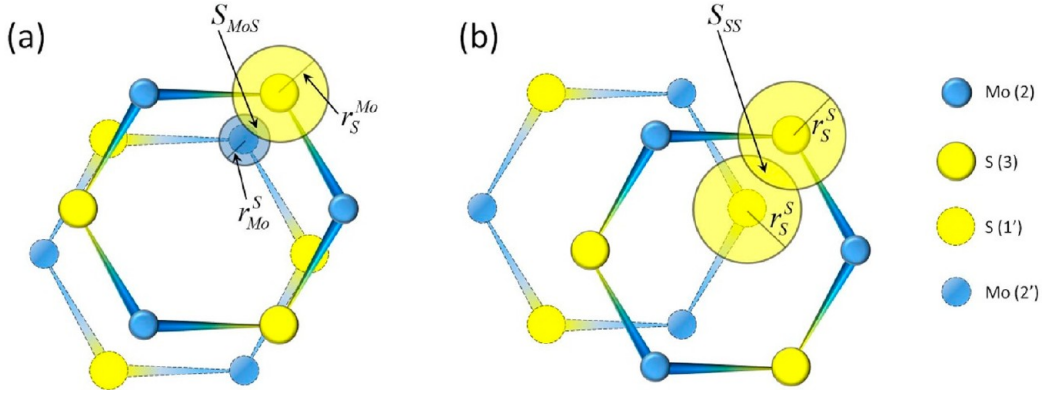

Figure 2. Projected circle overlaps used in the definition of the RI. (a) S_{MoS}- projected overlap between a circle of radius r_{Mo}^S centered on a Mo atom of one layer and a circle of radius r_S^{Mo} centered on a S atom of the adjacent layer. (b) S_{SS}-projected overlap between two circles of radii r_S^S centered on two S atoms belonging to adjacent layers.

position.[32,33] Here, the situation is somewhat more complex as each MoS_2 layer is composed of three parallel sublayers (see Figure 1). Therefore, the choice of circle radius has to reflect the distance between each pair of sublayers considered. To this end, we ascribe to each atomic position two radii representing the different interactions between sublayers 2,3 and 1′,2′, as described in Figure 1.[35] We mark these radii as r_α^β, where α is the atom around which the circle is centered and β is the corresponding atom on the other layer (see Figure 2). As will be shown below, in order to obtain optimal fitting with density functional theory (DFT) calculations, the following radii are chosen: r_S^S = 0.9 Å, r_S^{Mo} = 0.8 Å, and r_{Mo}^S = 0.3 Å.[36]

For the definition of the RI, the optimal and worst (in terms of energy) interlayer stacking modes have to be identified. The optimal (most energetically stable) interlayer configuration is known to be the AA′ stacking mode where S atoms of one layer reside atop Mo atoms of the other layer (see Figure 3a).[29] Starting from this configuration, the worst (highest in energy) laterally shifted interlayer configuration is the AB_2 stacking mode, where the positions of S atoms from both layers are fully

dx.doi.org/10.1021/jz300735v | J. Phys. Chem. Lett. 2012, 3, 1936−1940

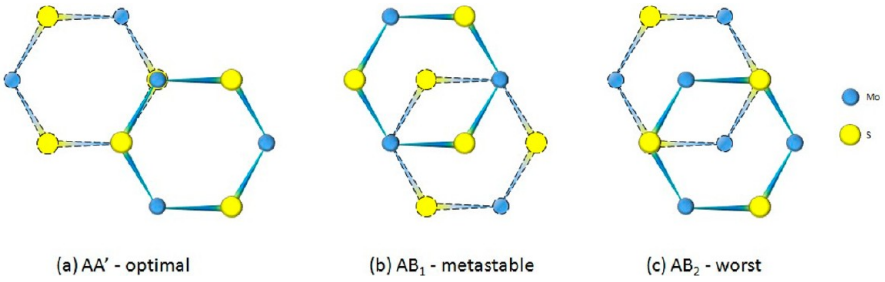

Figure 3. High-symmetry stacking modes of MoS_2. (a) AA′ configuration, the optimal stacking mode; (b) AB_1 configuration, a metastable stacking mode; (c) AB_2 configuration, the worst stacking mode.

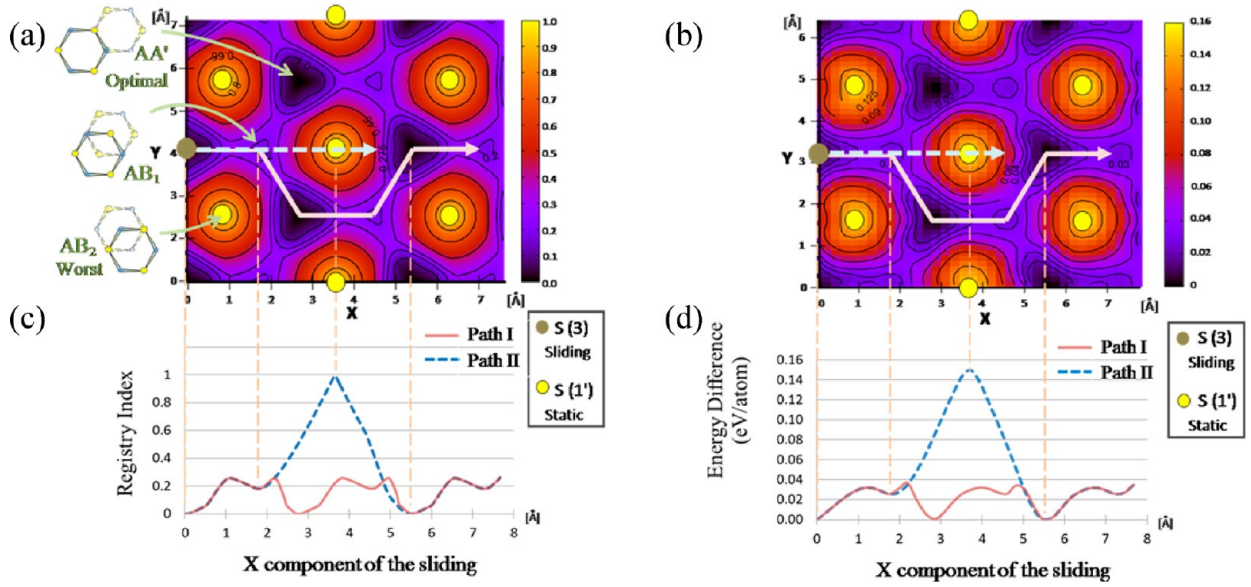

Figure 4. Interlayer sliding energy landscape of bilayer 2*H*-MoS_2. Top: (a) RI and (b) total DFT energy variations (eV/atom) as a function of lateral interlayer displacements in the *X*−*Y* plane. Bottom: (c) RI and (d) total DFT energy variations (eV/atom) along specific sliding pathways. DFT results, under an external pressure of 500 MPa, were reproduced with the kind permission and help of Prof. Simon R. Phillpot and his co-workers from ref 29. Copyright (2008) by the American Physical Society.

eclipsed and the Mo atoms reside above the centers of the hexagons of the adjacent layers (see Figure 3c). We note that the S−S overlap (S_{SS}; see Figure 2) is maximal at the worst stacking mode, whereas the Mo−S overlap (S_{MoS}; see Figure 2) is maximal at the optimal stacking mode. Since we would like the RI to be maximal at the worst staking mode and minimal and the optimal stacking mode, we set it to be proportional to the difference between the S−S and Mo−S overlaps, RI $\propto (S_{SS} - S_{MoS})$. Finally, normalizing this expression to the range [0:1] yields

$$\mathrm{RI} = \frac{(S_{SS} - S_{SS}^{AA'}) - (S_{MoS} - S_{MoS}^{AA'})}{(S_{SS}^{AB_2} - S_{SS}^{AA'}) - (S_{MoS}^{AB_2} - S_{MoS}^{AA'})}$$

where $S_{SS}^{AA'}$ and $S_{MoS}^{AA'}$ are the S−S and Mo−S overlaps at the AA′ stacking mode, respectively, and $S_{SS}^{AB_2}$ and $S_{MoS}^{AB_2}$ are the S−S and Mo−S overlaps at the AB_2 stacking mode, respectively.

Once we have a closed expression for the RI, we can calculate it for various interlayer configurations and compare the resulting RI surface to the sliding energy landscape obtained from DFT calculations. To this end, we construct a unit cell of bilayer 2*H*-MoS_2 using the lattice parameters of the bulk crystal (see Supporting Information). The unit cell of the lower layer is multiplied to form a sufficiently large finite sheet, and a single unit cell of the upper layer is then shifted with respect to the finite sheet to represent different relative interlayer positions. At each interlayer position, the RI is recalculated resulting in a full RI sliding surface.

In Figure 4, we present the main result of this study, where the sliding energy landscape obtained under an external pressure of 500 MPa using DFT calculations at the local density approximation level of theory[29] is compared with the predictions of the RI model. First, we consider the total RI landscape (Figure 4a) as compared to the full sliding energy surface obtained via the DFT calculations (Figure 4b). As can be seen, remarkable agreement between the two surfaces is achieved. The simple RI model is able to fully capture all important physical features appearing in the sliding energy landscape, including all stationary points that occur at high-symmetry interlayer configurations. By construction, the RI model correctly predicts the AA′ stacking mode to be the lowest-energy interlayer configuration and the AB_2 mode to be the highest-energy stacking mode. Furthermore, the AB_1 stacking mode, where the positions of Mo atoms from both layers are fully eclipsed and the S atoms reside at the centers of the hexagons of the adjacent layers (see Figure 3b), is found to be a local minimum on the RI landscape, in accordance with its metastable nature obtained via the DFT results. To better appreciate the agreement between the two calculations, we

dx.doi.org/10.1021/jz300735v | *J. Phys. Chem. Lett.* 2012, 3, 1936−1940

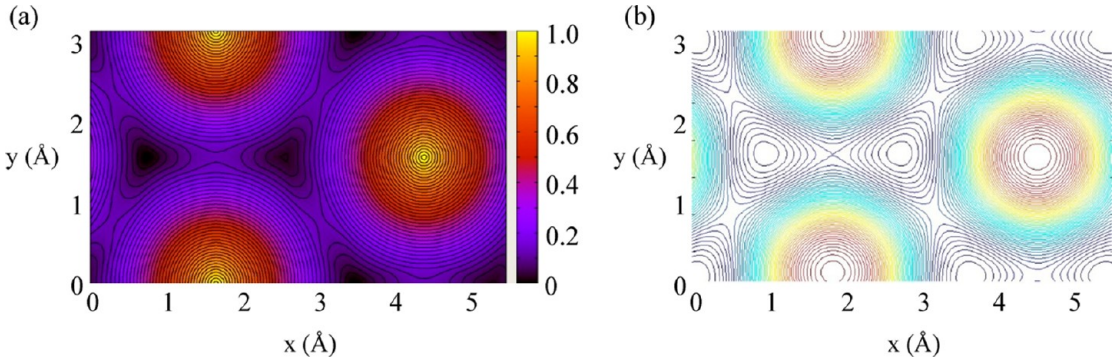

Figure 5. 2*H*-MoS_2 interlayer RI surface (a) tuned to match the DFT sliding energy landscape at an external pressure of 15 GPa (b). The overall corrugation of the DFT sliding energy landscape is ∼1 eV. DFT results were reproduced with the kind permission and help of Prof. S. Ciraci and his co-workers from ref 31. Copyright (2012) by the American Physical Society.

present in Figure 4c slices of the full RI landscape along specific pathways passing through the different surface minima and maxima. The choice of pathways was directed to match that presented in ref 29. For both paths considered, excellent agreement between the RI variations and the DFT energy changes (Figure 4d) is obtained.

The effect of external pressure on the sliding physics of 2*H*-MoS_2 can be evaluated by comparing the results presented above to recent DFT calculations of the sliding energy landscape of this material under an external pressure of 15 GPa.[31,37] At this higher external pressure, the repulsions between electron clouds of atoms belonging to two adjacent layers are considerably enhanced. As can be seen in Figure 5b, this is manifested in larger variations of the sliding energy landscape resulting in higher energetic barriers for interlayer sliding. Furthermore, the asymmetry observed between the AA′ and the AB_1 stacking modes at lower external pressure is almost completely removed in the higher-pressure calculation. Interestingly, by an appropriate choice of the circle radii, the RI landscape can be tuned to reproduce the higher-pressure calculations results (see Figure 5a). This exemplifies the flexibility of the RI method for describing the sliding physics in layered materials under different external conditions. Furthermore, comparing the radii of the different atomic circles used to reproduce the two DFT calculations provides insights regarding the origin of the effects of the external pressure on the overall sliding energy landscape. Specifically, to produce Figure 5, we keep r_S^S = 0.9 Å and reduce the other radii to r_S^{Mo} = 0.15 Å and r_{Mo}^S = 0.1 Å. This shows that upon increasing the external load, strong Pauli repulsions between the overlapping electron clouds of neighboring sulfur atoms on adjacent layers become the dominant factor determining the sliding energy landscape, whereas the interactions between the more remote S−Mo sublayers become relatively less important. This further explains the relative reduction in asymmetry between the AA′ and AB_1 stacking modes, where the leading interlayer terms result from S−Mo and Mo−Mo overlaps rather than the dominant S−S repulsions.

The notable agreement obtained between the RI results and more sophisticated first-principles calculations for 2*H*-MoS_2 further enhances our confidence that sliding energy landscapes of layered materials, however complex they may be, can be well-captured by simple models based on geometrical considerations. These, in turn, may provide an intuitive description of the physical processes underlying wearless friction in complex layered structures as well as an efficient means for modeling the tribological behavior of complex nanoscale material interfaces under various external conditions.

To summarize, in this work, we have defined the RI for layered metal dichalcogenides, focusing on the layered phase of MoS_2. Unlike the case of few layered graphene and hexagonal boron nitride,[32,33] where each layer is composed of a single flat sheet of atoms, 2*H*-MoS_2 has an intricate sublayer structure that reflects on its tribological properties. Despite the involved network of interlayer interactions between different sublayers, the RI is able to provide an accurate description of the interlayer sliding physics in 2*H*-MoS_2 at a fraction of the computational cost of first-principles calculations. On the basis of these results and the experience accumulated with the RI thus far, we believe that our suggested model can be applied for other members of the family of metal dichalcogenides, such as the layered phase of WS_2, and may also be expanded to describe their tubular counterparts.[32] The conclusions of the present work further affirm the robustness of the RI concept as an intuitive, flexible, and computationally efficient tool for studying nanoscale tribological characteristics of complex layered structures at the wearless friction regime.

■ ASSOCIATED CONTENT

Supporting Information

Partial coordinates representation of the natural 2*H*-MoS_2 unit cell and Cartesian coordinates of some of its high-symmetry interlayer stacking modes. This material is available free of charge via the Internet at http://pubs.acs.org.

■ AUTHOR INFORMATION

Corresponding Author

*E-mail: odedhod@tau.ac.il.

Author Contributions

†These authors contributed equally to this study.

Notes

The authors declare no competing financial interest.

■ ACKNOWLEDGMENTS

The authors would like to thank Prof. Simon R. Phillpot, Tao Liang, W. Gregory Sawyer, Scott S. Perry, and Susan B. Sinnott, from the Department of Materials Science and Engineering and the Department of Mechanical and Aerospace Engineering at University of Florida, Gainesville, U.S.A., for generously sharing the results of their DFT calculations[29] on which Figure 4b and 4d of this paper is based. We would further like to thank Prof. S. Ciraci, S. Cahangirov, C. Ataca, M. Topsakal, and H. Sahin

from UNAM-National Nanotechnology Research Center, the Institute of Materials Science and Nanotechnology, and the Department of Physics of Bilkent University, Ankara, Turkey, for generously sharing the results of their DFT calculations[31] on which Figure 5b of this paper is based. This work was supported by the Israel Science Foundation under Grant No. 1313/08, the Center for Nanoscience and Nanotechnology at Tel Aviv University, and the Lise Meitner-Minerva Center for Computational Quantum Chemistry.

REFERENCES

(1) Dienwiebel, M.; Verhoeven, G. S.; Pradeep, N.; Frenken, J. W. M.; Heimberg, J. A.; Zandbergen, H. W. *Phys. Rev. Lett.* **2004**, *92*, 126101.
(2) Hirano, M.; Shinjo, K. *Phys. Rev. B* **1990**, *41*, 11837.
(3) Shinjo, K.; Hirano, M. *Surf. Sci.* **1993**, *283*, 473.
(4) Nagapriya, K. S.; Goldbart, O.; Kaplan-Ashiri, I.; Seifert, G.; Tenne, R.; Joselevich, E. Torsional Stick−Slip Behavior in WS_2 Nanotubes. *Phys. Rev. Lett.* **2008**, *101*, 195501.
(5) Cohen-Karni, T.; Segev, L.; Srur-Lavi, O.; Cohen, S. R.; Joselevich, E. Torsional Electromechanical Quantum Oscillations in Carbon Nanotubes. *Nat. Nano* **2006**, *1*, 36−41.
(6) Stampfer, C.; Jungen, A.; Linderman, R.; Obergfell, D.; Roth, S.; Hierold, C. Nano-Electromechanical Displacement Sensing Based on Single-Walled Carbon Nanotubes. *Nano Lett.* **2006**, *6*, 1449−1453.
(7) Fennimore, A. M.; Yuzvinsky, T. D.; Han, W.-Q.; Fuhrer, M. S.; Cumings, J.; Zettl, A. Rotational Actuators Based on Carbon Nanotubes. *Nature* **2003**, *424*, 408−410.
(8) Peng, H. B.; Chang, C. W.; Aloni, S.; Yuzvinsky, T. D.; Zettl, A. Ultrahigh Frequency Nanotube Resonators. *Phys. Rev. Lett.* **2006**, *97*, 087203.
(9) Zheng, Q.; Jiang, Q. Multiwalled Carbon Nanotubes as Gigahertz Oscillators. *Phys. Rev. Lett.* **2002**, *88*, 045503.
(10) Cumings, J.; Zettl, A. Low-Friction Nanoscale Linear Bearing Realized from Multiwall Carbon Nanotubes. *Science* **2000**, *289*, 602−604.
(11) Forró, L. Beyond Gedanken Experiments. *Science* **2000**, *289*, 560−561.
(12) Grierson, D. S.; Carpick, R. W. Nanotribology of Carbon-Based Materials. *Nano Today* **2007**, *2*, 12−21.
(13) Sheehan, P. E.; Lieber, C. M. Nanotribology and Nanofabrication of MoO_3 Structures by Atomic Force Microscopy. *Science* **1996**, *272*, 1158−1161.
(14) Greenberg, R.; Halperin, G.; Etsion, I.; Tenne, R. The Effect of WS_2 Nanoparticles on Friction Reduction in Various Lubrication Regimes. *Tribol. Lett.* **2004**, *17*, 179−186.
(15) Rapoport, L. B., Y.; Feldman, Y.; Homyonfer, M.; Cohen, S. R.; Tenne, R. Hollow Nanoparticles of WS_2 as Potential Solid-State Lubricants. *Nature* **1997**, *387*, 791−793.
(16) Rapoport, L.; Fleischer, N.; Tenne, R. Fullerene-Like WS_2 Nanoparticles: Superior Lubricants for Harsh Conditions. *Adv. Mater.* **2003**, *15*, 651−655.
(17) Rapoport, L.; Leshchinsky, V.; Lvovsky, M.; Lapsker, I.; Volovik, Y.; Feldman, Y.; Popovitz-Biro, R.; Tenne, R. Superior Tribological Properties of Powder Materials with Solid Lubricant Nanoparticles. *Wear* **2003**, *255*, 794−800.
(18) Cizaire, L.; Vacher, B.; Le Mogne, T.; Martin, J. M.; Rapoport, L.; Margolin, A.; Tenne, R. Mechanisms of Ultra-Low Friction by Hollow Inorganic Fullerene-Like MoS_2 Nanoparticles. *Surf. Coat. Technol.* **2002**, *160*, 282−287.
(19) Cohen, S. R.; Feldman, Y.; Cohen, H.; Tenne, R. Nanotribology of Novel Metal Dichalcogenides. *Appl. Surf. Sci.* **1999**, *144−145*, 603−607.
(20) Cohen, S. R.; Rapoport, L.; Ponomarev, E. A.; Cohen, H.; Tsirlina, T.; Tenne, R.; Levy-Clement, C. The Tribological Behavior of Type II Textured MX_2 (M = Mo, W; X = S, Se) Films. *Thin Solid Films* **1998**, *324*, 190−197.
(21) Onodera, T.; Morita, Y.; Suzuki, A.; Koyama, M.; Tsuboi, H.; Hatakeyama, N.; Endou, A.; Takaba, H.; Kubo, M.; Dassenoy, F.; Minfray, C.; Joly-Pottuz, L.; Martin, J.-M.; Miyamoto, A. A Computational Chemistry Study on Friction of h-MoS_2. Part I. Mechanism of Single Sheet Lubrication. *J. Phys. Chem. B* **2009**, *113*, 16526−16536.
(22) Onodera, T.; Morita, Y.; Nagumo, R.; Miura, R.; Suzuki, A.; Tsuboi, H.; Hatakeyama, N.; Endou, A.; Takaba, H.; Dassenoy, F.; Minfray, C.; Joly-Pottuz, L.; Kubo, M.; Martin, J.-M.; Miyamoto, A. A Computational Chemistry Study on Friction of h-MoS_2. Part II. Friction Anisotropy. *J. Phys. Chem. B* **2010**, *114*, 15832−15838.
(23) Brown, S.; Musfeldt, J. L.; Mihut, I.; Betts, J. B.; Migliori, A.; Zak, A.; Tenne, R. Bulk vs Nanoscale WS_2: Finite Size Effects and Solid-State Lubrication. *Nano Lett.* **2007**, *7*, 2365−2369.
(24) Radisavljevic, B.; Radenovic, A.; Brivio, J.; Giacometti, V.; Kis, A. Single-Layer MoS2 Transistors. *Nat. Nano* **2011**, *6*, 147−150.
(25) Yoon, Y.; Ganapathi, K.; Salahuddin, S. How Good Can Monolayer MoS_2 Transistors Be? *Nano Lett.* **2011**, *11*, 3768−3773.
(26) Popov, I.; Seifert, G.; Tománek, D. Designing Electrical Contacts to MoS_2 Monolayers: A Computational Study. *Phys. Rev. Lett.* **2012**, *108*, 156802.
(27) Martin, J. M.; Donnet, C.; Le Mogne, T.; Epicier, T. Superlubricity of Molybdenum Disulphide. *Phys. Rev. B* **1993**, *48*, 10583−10586.
(28) Miura, K.; Kamiya, S. Observation of the Amontons−Coulomb Law on the Nanoscale: Frictional Forces Between MoS_2 Flakes and MoS_2 Surfaces. *Europhys. Lett.* **2002**, *58*, 610−615.
(29) Liang, T.; Sawyer, W. G.; Perry, S. S.; Sinnott, S. B.; Phillpot, S. R. First-Principles Determination of Static Potential Energy Surfaces for Atomic Friction in MoS_2 and MoO_3. *Phys. Rev. B* **2008**, *77*, 104105.
(30) Liang, T.; Phillpot, S. R.; Sinnott, S. B. Parametrization of a Reactive Many-Body Potential for Mo−S Systems. *Phys. Rev. B* **2009**, *79*, 245110.
(31) Cahangirov, S.; Ataca, C.; Topsakal, M.; Sahin, H.; Ciraci, S. Frictional Figures of Merit for Single Layered Nanostructures. *Phys. Rev. Lett.* **2012**, *108*, 126103.
(32) Hod, O. Quantifying the Stacking Registry Matching in Layered Materials. *Isr. J. Chem.* **2010**, *50*, 506−514.
(33) Marom, N.; Bernstein, J.; Garel, J.; Tkatchenko, A.; Joselevich, E.; Kronik, L.; Hod, O. Stacking and Registry Effects in Layered Materials: The Case of Hexagonal Boron Nitride. *Phys. Rev. Lett.* **2010**, *105*, 046801.
(34) Hod, O. Superlubricity — A New Perspective on an Established Paradigm. *arXiv:1204.3749* **2012**, submitted.
(35) The interactions with sublayers 1 and 3′ are neglected due to their relatively large distance and the expected screening effects induced by the inner layers.
(36) We find that the sliding physics is captured well without considering Mo−Mo overlap contributions; we therefore choose $r_{MO}^{MO} = 0$.
(37) We note that here we are comparing higher-pressure PBE results to lower-pressure LDA results. Nevertheless, the corrugation of the sliding energy landscape can be mainly attributed to Pauli repulsions between overlapping electron clouds of atoms belonging to two adjacent layers as they cross each other during the sliding process. These repulsions are well-captured by both functional approximations in the short−middle range regime, and therefore, the overall effect of the choice of functional approximation for the study of the sliding physics at such high external pressures is expected to be small.